Journal of Power Sources 269 (2014) 189–193

Contents lists available at ScienceDirect

Journal of Power Sources

journal homepage: www.elsevier.com/locate/jpowsour

Short communication

Tortuosity factor of three-dimensional infiltrate network

Yanxiang Zhang [a, b, c], Changrong Xia [b, 1], Fanglin Chen [c, *]

[a] National Key Laboratory for Precision Hot Processing of Metals, School of Materials Science and Engineering, Harbin Institute of Technology, Harbin 150001, China
[b] CAS Key Laboratory of Materials for Energy Conversion, Department of Materials Science and Engineering, University of Science and Technology of China, Hefei 230026, China
[c] Department of Mechanical Engineering, University of South Carolina, Columbia, SC 29205, United States

HIGHLIGHTS

- Tortuosity factor of the 3D infiltrate network is calculated.
- Analytical model for the tortuosity factor of infiltrate network is developed.
- Strategies to decrease the tortuosity factor of infiltrate network are suggested.
- Intrinsic conductivity of the infiltrate network can be resolved.

ARTICLE INFO

Article history:
Received 28 April 2014
Received in revised form
24 June 2014
Accepted 25 June 2014
Available online 7 July 2014

Keywords:
Tortuosity
Infiltration
Model
Nanostructure
Solid oxide cell
Electrode

ABSTRACT

The tortuosity factor is calculated by solving Laplace's equation of electrostatic potential within the numerically constructed three-dimensional infiltrate network of nanostructured solid oxide cell electrodes. Based on Bruggeman approach, an analytical model is proposed to calculate the tortuosity factor and effective conductivity as a function of infiltration loading. The intrinsic conductivity of infiltrate network can be resolved from its effective conductivity using the analytical model. Good agreement is found between the numerical and analytical models and the experimental data in literature. Parametric study for the effects of backbone microstructure, nanoparticle size and aggregation of infiltrate suggests practical strategies to decrease the tortuosity factor of infiltrate network.

1. Introduction

Nanostructured engineering has drawn tremendous attention to prepare highly active electrodes for solid oxide cells (SOCs) [1–3] and gas separation membranes [4]. Infiltration is the most widely utilized method to increase electrode performance by introducing nano-scale geometric features where electrochemical reactions take place. For specific material systems, numerous SOCs with the highest power density or the lowest polarization resistance have been reported by using infiltration [1,5]. Modeling and experimental studies have tried to link the performance with the geometric factors of infiltrated electrodes. For instance, the Surface Resistance model [6] and the modified model [7] calculate the polarization resistance of mixed ionic electronic conductor (MIEC) infiltrated ionic conductor electrodes as a function of MIEC surface area; The Particle Layer model links three-phase boundary length with the polarization resistance of the electronic conductor infiltrated ionic conductor electrodes [8]. However, many details of infiltrated electrodes remain a mystery. One important issue is the effective conductivity of the infiltrate network [9],

$$\sigma_{\text{eff}} = \frac{\phi}{\tau}\sigma_0 \tag{1}$$

where σ_0 is the intrinsic conductivity of infiltrate network; τ is the tortuosity factor; and ϕ is infiltration loading (volume fraction of infiltrate in the entire electrode including pores). Experimental observations show that the electronic conductivity of electrode can be increased significantly by a small loading of electronic infiltrate

* Corresponding author. Tel.: +1 803 777 4875; fax: +1 803 777 0106.
E-mail addresses: xiacr@ustc.edu.cn (C. Xia), chenfa@cec.sc.edu (F. Chen).
[1] Tel.: +86 551 3607475; fax: +86 551 3601592.

http://dx.doi.org/10.1016/j.jpowsour.2014.06.141
0378-7753/

(e.g. 5 vol.%), however, can not be further promoted to a high level comparable to that of the conventional composite electrodes [10,11]. This can be attributed to either or both of the high tortuosity factor and the low intrinsic conductivity. However, the contributions of geometric properties (τ) and materials properties (σ_0) can not be well separated yet. This is partially because of the challenges in the quantification of electrode microstructures. Scanning electron microscopy (SEM) has been used to estimate infiltrated nanoparticle size [7,12]. Advanced techniques such as focused ion beam − SEM and X-ray computed tomography have been used to quantify the 3D geometric factors such as percolation properties and tortuosity factors for conventional composite electrodes [13,14]. However, it is challenging to capture the nano-scale features of infiltrated electrodes due to the limited resolution (10–50 nm). Recently, Kishimoto et al. utilized high-resolution focused ion beam tomography and for the first time reconstructed the 3D microstructure of an infiltrated electrode [15]. In this work, we construct the 3D microstructures of infiltrated electrodes by using the numerical infiltration methodology of our previous work [16]. Then, the tortuosity factor of the infiltrate network is calculated by solving Laplace's equation for charge transport within the 3D network. Effects of backbone microstructure, nanoparticle size and aggregation of infiltrate are studied. Analytical model is developed for the tortuosity factor and effective conductivity, and verified by both the numerical and experimental results.

2. Numerical methodology

The most common infiltration process involves depositing a catalyst precursor solution of metal nitrates into an existing porous backbone, followed by firing at 800–900 °C to form the catalyst nanoparticles. In our previous study, a numerical methodology has been developed to simulate the 3D microstructures of infiltrated electrodes [16]. The numerical procedure consists of two steps. The first step is to generate backbone matrix by randomly dropping spherical particles with an intended contact angle within a 3D empty domain, which is discretized into voxels. This work still employs the 1000 nm × 1000 nm × 1000 nm domain with a spatial resolution of 5 nm, which has been verified to be sufficient to represent the infiltrated nano-scale microstructures [16]. The second step is to randomly fit nanoparticles with intended contact angles onto the surface of the generated backbone matrix one by one. The probability for each nanoparticle coating onto the backbone surface is defined as,

$$P_{\mathrm{BBS}} = w\mathrm{Area}_{\mathrm{BBS}}/[w\mathrm{Area}_{\mathrm{BBS}} + (1-w)\mathrm{Area}_{\mathrm{NPS}}] \quad (2)$$

where $\mathrm{Area}_{\mathrm{BBS}}$ [μm^2 μm^{-3}] is the backbone surface area after infiltration; $\mathrm{Area}_{\mathrm{NPS}}$ [μm^2 μm^{-3}] is the nanoparticles surface area; w is a weighting parameter, in the range of 0–1. Otherwise, the nanoparticle is coated onto the existing nanoparticle surface to simulate the aggregation of nanoparticles.

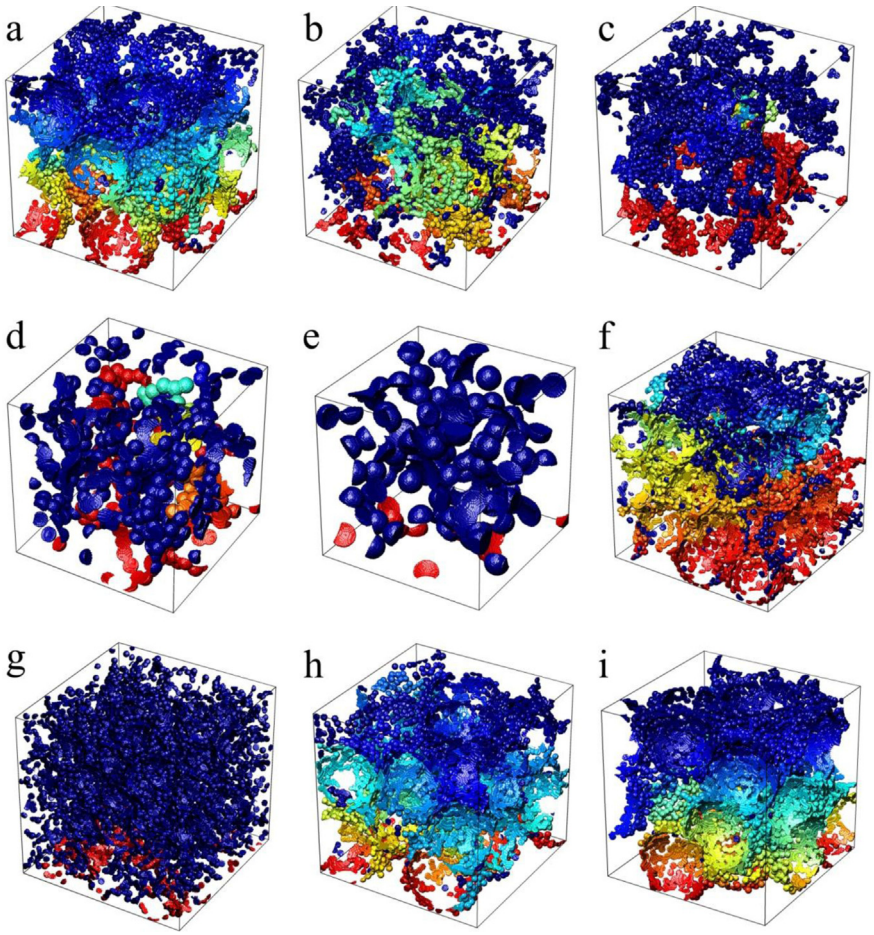

Fig. 1. Visualization of the infiltrate networks with a infiltrate loading of 10 vol.%. Domain side length is 1000 nm with a resolution of 5 nm. Colors from red to blue proportionally represent the electric potential from 1 V to 0 V. (a) The baseline condition with $w = 0.9$, $r_{\mathrm{NP}} = 25$ nm, $r_{\mathrm{BB}} = 200$ nm, and $\phi_{\mathrm{BB}} = 0.5$. b and c show the effects of w, which is 0.5 and 0.1 respectively; d and e show the effects of r_{NP}, 50 nm and 75 nm; f and g show the effects of r_{BB}, 150 nm, and 100 nm; h and i show the effects of ϕ_{BB}, 40 vol.% and 60 vol.%. (For interpretation of the references to color in this figure legend, the reader is referred to the web version of this article.)

a

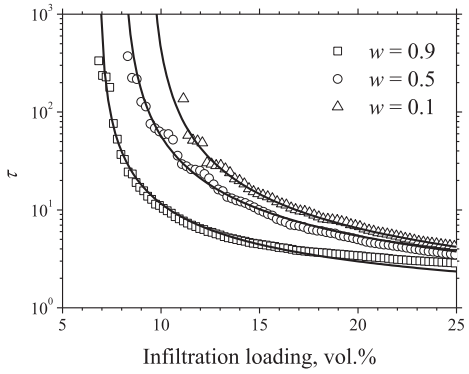

b

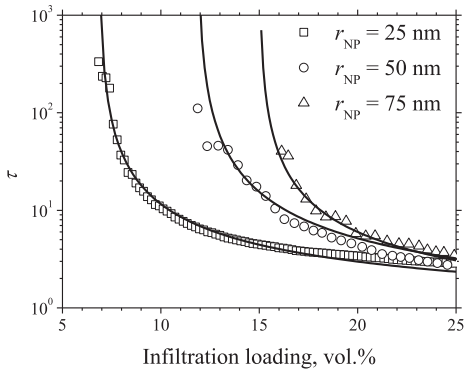

c

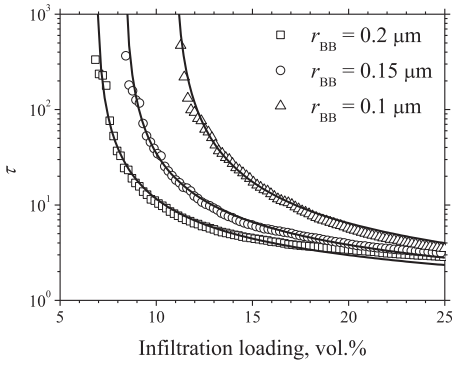

d

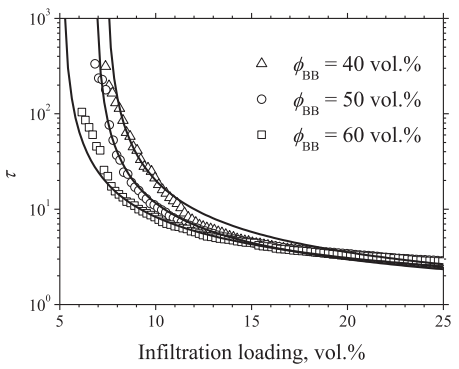

During the numerical infiltration procedure, the tortuosity factor of the 3D nanoparticles network is calculated as [9],

$$\tau = \phi\sigma_0 \Big/ \sigma_{\text{eff}} \tag{3}$$

Eq. (3) indicates that $\sigma_0/\sigma_{\text{eff}}$ should be a constant. Theoretically, $\sigma_0/\sigma_{\text{eff}}$ can be 'measured' numerically by solving Laplace's equation for charge transport within the 3D infiltrate network,

$$\Delta\psi = 0 \tag{4}$$

where ψ stands for the electrostatic potential. To avoid singularity, the isolate nanoparticle clusters are excluded. Electrostatic potentials of ψ_0 and ψ_1 are enforced on the top and bottom boundaries of the infiltrated network, respectively. Then the conductivity ratio is estimated as,

$$\frac{\sigma_0}{\sigma_{\text{eff}}} = \frac{\psi_1 - \psi_0}{d}\frac{A}{\iint_S \nabla\psi \mathrm{d}S} \tag{5}$$

where d is the distance between the top and the bottom boundaries, 1000 nm; A is the surface area of the entire top boundary, 10^6 nm^2; S is the surface area of infiltrate on the top boundary. Eqs. (4) and (5) are solved by in-house MATLAB code.

3. Analytical model for tortuosity factor

The effective conductivity of porous network is usually modeled by the empirical Bruggeman relationship [17],

$$\sigma_{\text{eff}} = \phi^{\mu}\sigma_0 \tag{6}$$

where μ is the Bruggeman factor. We assume the infiltrate network obeys Eq. (6). It is noted that the infiltrate network is conductive only when the volume fraction is above percolation threshold, ϕ_c. On the other hand, the maximum infiltration loading is the backbone porosity, ϕ_{BB}, in other words, the maximum conductivity of the infiltrated network corresponds to the effective conductivity when the pores are fully infiltrated, σ_{pore}. Accordingly, it is natural to rescale the volume fraction in Eq. (6) in the range between ϕ_c and ϕ_{BB},

$$\sigma_{\text{eff}} = \left[\frac{\phi - \phi_c}{\phi_{BB} - \phi_c}\right]^{\mu}\sigma_{\text{pore}} \tag{7}$$

where the maximum conductivity is given by,

$$\sigma_{\text{pore}} = \phi_{BB}^{\mu}\sigma_0 \tag{8}$$

Inserting Eq. (8) into Eq. (7), we can obtain the effective conductivity,

$$\sigma_{\text{eff}} = \left[\phi_{BB}\frac{\phi - \phi_c}{\phi_{BB} - \phi_c}\right]^{\mu}\sigma_0 \tag{9}$$

Combining Eq. (3) with Eq. (9), the tortuosity factor of infiltrated network can be estimated as,

$$\tau = \phi\left(\phi_{BB}\frac{\phi - \phi_c}{\phi_{BB} - \phi_c}\right)^{-\mu} \tag{10}$$

Bruggeman factor is treated as a fitting parameter.

Fig. 2. Tortuosity factor of infiltrate networks as a function of infiltration loading. The effects of w, r_{NP}, r_{BB} and ϕ_{BB} are shown in (a–d), respectively. Scatters are numerical results and solid lines are the fitting of Eq. (10).

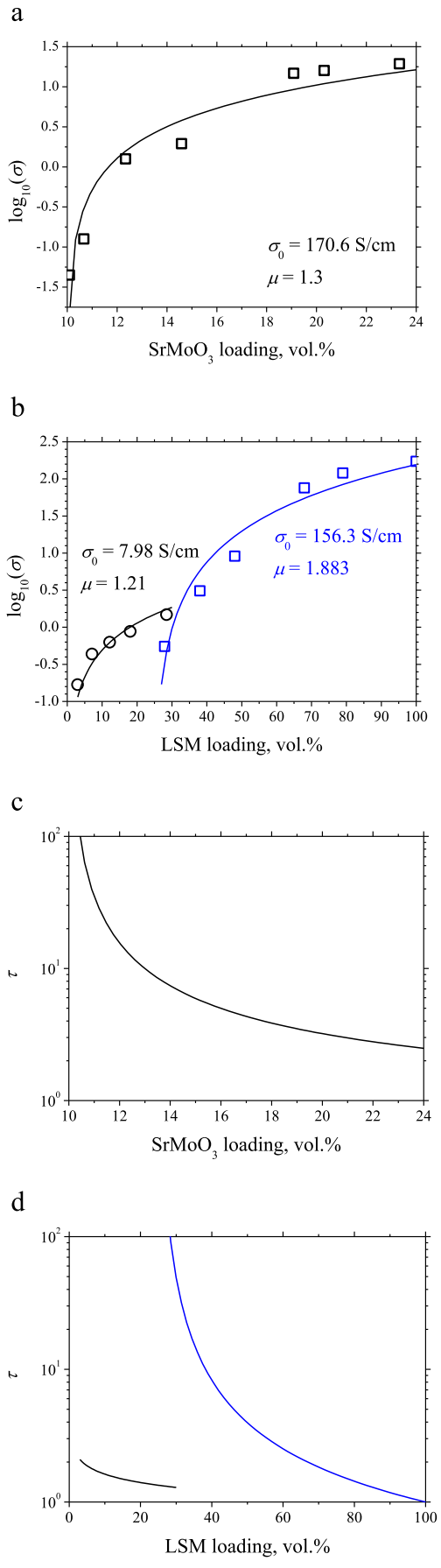

4. Results and discussion

The tortuosity factor of infiltrated network is calculated as a function of infiltration loading. Morphology of the infiltrated network is governed by four factors – the aggregation risk of nanoparticles, nanoparticle radius, backbone particle radius, and backbone porosity. Thus, the effects of these four factors are studied. A baseline condition is defined as $w = 0.9$, $r_{NP} = 25$ nm, $r_{BB} = 200$ nm, and $\phi_{BB} = 0.5$. And the parametric study is conducted by changing one factor, while keeping the other factors unchanged.

Fig. 1 shows the electrostatic potential distribution within the 10 vol.% infiltrated networks under various conditions. Colors scale with electric potential from 1 V (red) to 0 V (blue). As is shown, when the weighting parameter decreases from the baseline 0.9 (Fig. 1a) to 0.5 (Fig. 1b) and 0.1 (Fig. 1c), the infiltrated nanoparticles tend to form aggregates, leading to insufficient connection between nanoparticles. Comparing with the baseline condition, the electric potential for $w = 0.5$ is badly distributed, in other words, the potential is not smoothly evolved from the bottom side to the top side. According to Ohm's law, the gradient of potential is proportional to current. Thus, the equipotential clusters in Fig. 1b and c do not contribute to the current transport, increasing the tortuosity. When the nanoparticle radius is increased to 50 nm (Fig. 1d) and 75 nm (Fig. 1e), the network is isolated under the infiltration loading of 10 vol.%, and thus leading to infinite tortuosity. Decreasing the backbone particle radius from baseline 200 nm–150 nm (Fig. 1f) deteriorates the potential distribution. The infiltrated network is isolated by decreasing backbone particle radius to 100 nm (Fig. 1g). The potential is badly distributed by decreasing backbone porosity from 60 vol.% (Fig. 1i) to baseline 50 vol.% (Fig. 1a) and 40 vol.% (Fig. 1h).

Fig. 2 shows the tortuosity factor evolution with infiltration loading under various conditions, revealing that the tortuosity factor decreases with increase in infiltration loading. For a given loading level, the tortuosity factor is decreased by increasing weighting factor (decreasing aggregation risk, Fig. 2a), decreasing infiltrated nanoparticle size (Fig. 2b), and/or increasing backbone particle size (Fig. 2c), consistent with Fig. 1. Increasing backbone porosity (Fig. 2d) can also decrease tortuosity factor but only slightly. Eq. (10) fits well to the numerical construction results. The Bruggeman factors under various conditions are in a range of 1.3–1.7, close to the typical value of 1.5 for the oft-used Bruggeman approaches [14].

The analytical model (Eq. (9)) is then fitted with literature data. Fig. 3 a and b show the fitting results of effective electronic conductivity of $SrMoO_3$ infiltrated network [10] and LSM infiltrated network [11] as a function of infiltration loading, showing that Eq. (9) agrees well with the literature data. The Bruggeman factors for $SrMoO_3$ infiltrate and LSM infiltrate are fitted as 1.3 and 1.21, respectively. They are similar to that of the numerical results. However, the fitted intrinsic conductivities, σ_0 for the infiltrated networks are significantly lower than that of the bulk materials. The intrinsic conductivity for $SrMoO_3$ infiltrate network is fitted as 170.6 S cm^{-1} at 800 °C, remarkably lower than that of the bulk $SrMoO_3$ material, about 10^3S/cm [10]. In comparison to the bulk LSM data (as the blue line shown in Fig. 3b), the fitted intrinsic conductivity for LSM infiltrate network is a factor of 20 times lower.

Fig. 3. Evolutions of electronic conductivities of (a) $SrMoO_3$ infiltrated YSZ anode at 800 °C in 97%H_2 + 3%H_2O, and (b) LSM infiltrated YSZ cathode (black) and LSM - YSZ composite cathode (blue) at 700 °C in air. Scatters are literature data [8,9] and lines are fitting results of Eq. (9). (c) and (d) show the calculated tortuosity factor of $SrMoO_3$ and LSM networks, respectively. (For interpretation of the references to color in this figure legend, the reader is referred to the web version of this article.)

The low intrinsic conductivity of infiltrate network may be caused by the blocking effects of grain boundaries and the impurity of infiltrate [18]. Although it is difficult to measure the intrinsic conductivity of infiltrate network, we may get some insights from the model. When the infiltration loading is near percolation threshold, the tortuosity factor is very high, and thus dominates the effective conductivity. However, for typical infiltration loadings, say 10–20 vol.%, the tortuosity factor becomes quite small. Fig. 3c and d shows the calculated tortuosity factor for the $SrMoO_3$ infiltrate and LSM infiltrate, which is 3 and 1.5 at 20 vol.% loading, respectively. In this case, the effective electronic conductivity of infiltrate network may be dominated by its intrinsic conductivity. On the other hand, it should be noted that the model will always overestimate the effective electronic conductivity of infiltrate network if one use the intrinsic conductivity of the bulk material instead of that for infiltrate network.

5. Conclusions

The numerical and analytical models show that the tortuosity factor of infiltrated nanoparticles network can be decreased by increasing infiltration loading, backbone particle size, backbone porosity, and/or by decreasing aggregation of nanoparticles, and infiltrated nanoparticle size. The tortuosity factor is very high ($>10^2$) near the percolation threshold, while quite small (<3) at typical infiltration loadings. By fitting the model to literature data, the intrinsic electronic conductivities of LSM and $SrMoO_3$ infiltrate networks are found to be significantly lower than that of the bulk materials.

Acknowledgments

We acknowledge the financial support from the Ministry of Science and Technology of China (2012CB215403) and the U.S. National Science Foundation (DMR-1210792).

References

[1] S.P. Jiang, Int. J. Hydrogen Energy 37 (2012) 449–470.
[2] Y. Chen, Y. Lin, Y. Zhang, S. Wang, D. Su, Z. Yang, M. Han, F. Chen, Nano Energy 8 (2014) 25–33.
[3] D. Ding, M. Liu, Z. Liu, X. Li, K. Blinn, X. Zhu, M. Liu, Adv. Energy Mater. 3 (2013) 1149–1154.
[4] A. Julbe, D. Farrusseng, C. Guizard, J. Membr. Sci. 181 (2001) 3–20.
[5] D. Ding, X. Li, S.Y. Lai, K. Gerdes, M. Liu, Energy Environ. Sci. 7 (2014) 552–575.
[6] M. Shah, J.D. Nicholas, S.A. Barnett, Electrochem. Commun. 11 (2009) 2–5.
[7] J.D. Nicholas, L. Wang, A.V. Call, S.A. Barnett, Phys. Chem. Chem. Phys. 14 (2012) 15379–15392.
[8] Y. Zhang, C. Xia, J. Power Sources 195 (2010) 4206–4212.
[9] Y. Zhang, C. Xia, M. Ni, Int. J. Hydrogen Energy 37 (2012) 3392–3402.
[10] B.H. Smith, M.D. Gross, Electrochem. Solid State Lett. 14 (2011) B1–B5.
[11] H. He, Y. Huang, J. Regal, M. Boaro, J.M. Vohs, R.J. Gorte, J. Am. Ceram. Soc. 87 (2004) 331–336.
[12] Z. Zhan, D.M. Bierschenk, J.S. Cronin, S.A. Barnett, Energy Environ. Sci. 4 (2011) 3951–3954.
[13] J.R. Wilson, W. Kobsiriphat, R. Mendoza, H.-Y. Chen, J.M. Hiller, D.J. Miller, K. Thornton, P.W. Voorhees, S.B. Adler, S.A. Barnett, Nat. Mater. 5 (2006) 541–544.
[14] J.R. Izzo, A.S. Joshi, K.N. Grew, W.K.S. Chiu, A. Tkachuk, S.H. Wang, W. Yun, J. Electrochem. Soc. 155 (2008) B504–B508.
[15] M. Kishimoto, M. Lomberg, E. Ruiz-Trejo, N.P. Brandon, J. Power Sources 266 (2014) 291–295.
[16] Y. Zhang, Q. Sun, C. Xia, M. Ni, J. Electrochem. Soc. 160 (2013) F278–F289.
[17] D.H. Jeon, J.H. Nam, C.-J. Kim, J. Electrochem. Soc. 153 (2006) A406–A417.
[18] J.M. Vohs, R.J. Gorte, Adv. Mater. 21 (2009) 943–956.